

Designing Waveforms with Adjustable PAPR for Integrated Sensing and Communication

Ahmad Bazzi*[†] and Marwa Chafii*[†]

*Engineering Division, New York University (NYU), Abu Dhabi, UAE.

[†]NYU WIRELESS, NYU Tandon School of Engineering, New York, USA

Abstract—This paper presents a new optimization framework dedicated for integrated sensing and communication (ISAC) waveform design. In particular, the problem aims at maximizing the total achievable sum-rate, through multi-user interference minimization, while preserving a certain level of similarity to a given desired radar waveform. Aiming towards feasible and practical PHY architectures, we also offer the flexibility of tuning the peak-to-average power ratio to a desired level. Towards this design, a non-convex optimization problem is formulated, and an alternating direction method of multipliers based solution is derived to converge towards the superiority of the final ISAC waveform. Finally, simulation results validate the proposed ISAC waveform design, as compared to state-of-the-art solutions.

Index Terms—6G, ISAC, PAPR, DFRC, waveform design

I. INTRODUCTION

Researchers have started to explore higher frequency ranges, spanning 300GHz to 3THz [1] to realize new technologies. In fact, one of the key ingredients of next generation wireless communication networks 6G mobile radio is integrated sensing and communication (ISAC) [2]. Indeed, ISAC strengthens high-quality wireless connectivity with support to high data transmission rates and accurate sensing features [3]. Therefore, diligence during the waveform design process is required to achieve such robustness in sensing, as well as high quality of communication [4]. Owing to its dual nature, ISAC architectures come with a handful of merits, such as hardware efficiency and shared resources [5].

ISAC can be split into three broad categories, where the first aims at a *joint design*, offering trade-offs between sensing and communications. For instance, [6] derives beamforming matrices for ISAC systems, in situations of imperfect channel state information, while [7] considers a joint design for variable length time snapshots. Another category is *communication-centric* ISAC, where one simply performs sensing using a known communication waveform, such as orthogonal frequency-division multiplexing (OFDM). The priority in this case is communications, and sensing comes as an add-on. This is interesting in applications where the communication infrastructure is established and follows a certain standard, ex. IEEE 802.11aj. For example, the novel design in [8] makes use of already-existing communication signals to perform sensing in a hybrid fashion and [9] utilizes an intelligent reflecting surface (IRS) to significantly enhance sensing performances. Furthermore, *radar-centric* ISAC’s main goal is to embed communication information onto a radar waveform.

See [10] for chirp waveforms conveying communication information. Now, we state some state-of-the-art methods related to ISAC waveform designs. Also, the work in [11] discusses a possible ISAC demonstration testbed for millimeter-wave applications.

The work in [12] focuses on spatial beamforming for the radar sub-system, whereas our work considers similarity constraints relative to a chirp with good auto-correlation properties, such as good ambiguity function properties, which further empower good time of arrival (ToA) estimations [13] via the received radar echo. Moreover, the work in [12] examines waveforms for multiple-input, multiple-output (MIMO)-OFDM intended for dual-functional radar and communication (DFRC) systems. In addition, the problem in [12] considers a weighted combination of communication and radar metrics. Unlike [12], we optimize the multi-user interference, under a chirp similarity constraint for the radar performance, subject to peak-to-average power ratio (PAPR) constraints and under an available power budget. Furthermore, the work in [14] uses convex optimization tools to derive an iterative clipping and filtering in the frequency domain. However, [14] does not enforce any multi-user communication metrics and radar metrics, but instead focuses on an OFDM symbol level to minimize its error vector magnitude (EVM). Waveform design based on constant modulus was proposed in [15] for MIMO radar, where the sequential optimization algorithm was adopted as a solution to the proposed framework. Even though the approach in [15] takes into account radar, as well as PAPR considerations [16], the approach does not account for multi-user communications. Similarly, a space-time coded design was adopted in [17] and a Dinkelbach-Type algorithm [18] was used as a solver towards their approach. Similar to [15], the approach in [17] lacks multi-user communication capabilities. From a DFRC perspective, the constant modulus design in [19] addresses multi-user communication and radar problem through the so-called branch and bound (BnB) method [20], thus guaranteeing a constant modulus waveform. Even though the solution is attractive in terms of PAPR, it lacks flexibility in yielding a desired PAPR. In many applications, the input back-off (IBO) of the high power amplifier (HPA), which is basically the operating point of the amplifier backed-off from the saturation level, is directly related to the nominal transmit PAPR. Therefore, in applications where IBO can have margin, the design in [19] does not seem to be well-suited as it does not utilize the available power margin. Moreover,

phase coded designs for radar performance is studied in [21] in order to maximize the radar's detection probability, but neither the PAPR nor the multi-communication performances were addressed.

In this paper, we address ISAC waveform design from a practical point of view. We first propose an ISAC waveform optimization framework, capable of multi-user interference minimization, while guaranteeing a similarity constraint relative to a radar chirp waveform. In addition, we take into account a practical factor, which is the PAPR of the transmit waveform. The proposed design is capable of tuning the PAPR to a desired level, a desired feature in practical PHY layer architectures. In principle, the general optimization framework falls under the class of multi-objective optimization (MOO), due to the various objectives involved in the problem [22]. After forming an equivalent non-convex optimization problem, we employ an alternating direction method of multipliers (ADMM) based solution to converge towards an ISAC waveform with desired PAPR and radar properties. Finally, we highlight the various benefits of the proposed waveform design and the capability of the ADMM-based waveform design solution in both radar sensing and multi-user communications, we present extensive simulation results showing the potential and superiority of the proposed design, when compared to state-of-the-art designs.

The remainder of this work is structured as follows. Section II introduces the sensing and communication system models. The key performance indicators (KPIs) used in this paper are given in Section III. Section IV introduces the ISAC waveform design framework and formally states the optimization problem addressed in this paper. In Section V, the iterative solution in solving the problem is derived. Simulation results are demonstrated in Section VI. Finally, we conclude the paper in Section VII.

Notation: Upper-case and lower-case boldface letters denote matrices and vectors, respectively. $(\cdot)^T$, $(\cdot)^*$ and $(\cdot)^H$ represent the transpose, the conjugate and the transpose-conjugate operators. The statistical expectation is $\mathbb{E}\{\cdot\}$. For any complex number $z \in \mathbb{C}$, the magnitude is $|z|$, its real part is $\text{Re}(z)$, and its imaginary part is $\text{Im}(z)$. For compactness, we denote the i^{th} row of matrix \mathbf{A} as \mathbf{A}_i . The Frobenius norm of matrix \mathbf{X} is $\|\mathbf{X}\|$. The matrix \mathbf{I}_N is the identity matrix of size $N \times N$. In particular, vec takes an $N \times M$ matrix \mathbf{X} as input and returns an $NM \times 1$ vector, by stacking the columns of \mathbf{X} . The inverse of a square matrix is \mathbf{X}^{-1} . We index the $(i, j)^{\text{th}}$ entry of matrix \mathbf{A} as $\mathbf{A}_{i,j}$. The all-ones vector of size N is denoted as $\mathbf{1}_N$ and \mathbf{o}_k is an all-zeros vector, except for its k^{th} entry, which is set to 1. The Kronecker product is denoted as \otimes . The value at the m^{th} iteration of a quantity, say x , involved in an iterative-type algorithm is denoted as $x^{(m)}$. The zero-vector is $\mathbf{0}$. Furthermore, the vectorization and unvectorization operators are denoted as vec and vec^{-1} , respectively.

II. SYSTEM MODEL

Let us consider a colocated mono-static DFRC base station (BS) equipped with N antennas in an arbitrary fashion. Also,

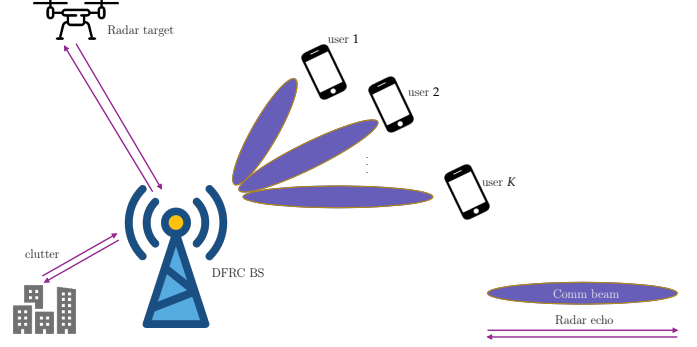


Fig. 1. An ISAC architecture, where the scenario consists of a target of interest, K communication users, and clutter due to scatterers in the environment.

consider a planar wave-front in signal propagation. The array steering vector of the antenna array at the DFRC BS is denoted by $\mathbf{a}(\theta)$ where θ is the angle of arrival (AoA) of the wavefront. An example is the uniform linear antenna array (ULA) configuration, where

$$\mathbf{a}(\theta) = \left[1, e^{-j \frac{2\pi d}{\lambda} \sin(\theta)}, \dots, e^{-j(N-1) \frac{2\pi d}{\lambda} \sin(\theta)} \right]^T, \quad (1)$$

where d is the inter-element spacing and λ is the wavelength. Communication users are considered to be located at random positions, whereas the target is supposed to be at a given angle θ_0 from the DFRC base station. Fig. 1 depicts a DFRC base station broadcasting the same ISAC signal, hereby denoted as $\mathbf{X} \in \mathbb{C}^{N \times L}$ (where L is the number of time samples), towards K communication users and an intended target of interest.

A. Sensing Echo Model

The ISAC DFRC BS is capable of sensing the desired echo signal, which refers to its own echo signal reflected off intended targets. Moreover, the echo signal encompasses the echo signal reflected by scatterers, referred to as environment clutter, and the echo signal reflected by targets of interest. Then, the received signal at the DFRC BS is as follows

$$\mathbf{Y}_r = \gamma_0 \mathbf{a}(\theta_0) \mathbf{a}^T(\theta_0) \mathbf{X} + \sum_{c=1}^C \gamma_c \mathbf{a}(\theta_c) \mathbf{a}^T(\theta_c) \mathbf{X} + \mathbf{Z}_r \in \mathbb{C}^{N \times L}. \quad (2)$$

The line-of-sight (LoS) component towards the target of interest is captured in $\gamma_0 \mathbf{a}(\theta_0) \mathbf{a}^T(\theta_0) \mathbf{X}$, where γ_0 is the reflection coefficient containing attenuation of the LoS component, as well as delay-doppler information within its phase. The AoA of the target is θ_0 . Moreover, we consider C clutter components, where the contribution of the c^{th} scatterer is expressed by the term $\gamma_c \mathbf{a}(\theta_c) \mathbf{a}^T(\theta_c) \mathbf{X}$. Furthermore, due to the colocated mono-static architecture, the shared crystal clock at the DFRC BS leads to perfect synchronization between its uplink (UL)/downlink (DL) sense, therefore, the carrier frequency offset (CFO) and the timing offset are zero [23]. Also, we assume that the above reception, sampling and signal processing occur during a time interval termed the

coherent processing interval (CPI) [6] which is an interval where sensing parameters are constant. Last but not least, the matrix \mathbf{Z}_r reflects zero-mean background noise at the radar sub-system, where each column is assumed to be independent from the other.

B. Communication DL Model

Using the same transmission, to leverage system resource, a single transmission in the DL sense, can be expressed as

$$\mathbf{Y}_c = \mathbf{H}\mathbf{X} + \mathbf{Z}_c \in \mathbb{C}^{K \times L}, \quad (3)$$

where the k^{th} row of \mathbf{Y}_c is the received vector at the k^{th} communication user. The channel matrix is given by $\mathbf{H} = [\mathbf{h}_1 \ \mathbf{h}_2 \ \dots \ \mathbf{h}_K]^T \in \mathbb{C}^{K \times N}$, and is flat Rayleigh type fading, assumed to be constant during one transmission. Additionally, the BS assumed complete channel knowledge \mathbf{H} . Finally, the vector $\mathbf{Z}_c \in \mathbb{C}^{K \times L}$ is background noise, where each column is white Gaussian i.i.d with zero mean and a multiple of identity covariance matrix as $\mathcal{N}(0, \sigma_c^2 \mathbf{I}_K)$.

III. KEY PERFORMANCE INDICATORS

It is critical to specify KPIs pertinent to the current system model in order to develop an appropriate and reliable optimization problem that attempts to solve ISAC difficulties. We can rewrite the received signal as equation (3) based on

$$\mathbf{Y}_c = \mathbf{S} + \underbrace{\mathbf{H}\mathbf{X} - \mathbf{S}}_{\text{MUI}} + \mathbf{Z}_c, \quad (4)$$

where MUI is multi-user interference and $\mathbf{S} \in \mathbb{C}^{K \times L}$ is the desired signal carrying information symbols. Following [24], it can be shown that the SINR at the k^{th} user can be represented as a function of MUI as

$$\text{SINR}_k = \frac{\mathbb{E}(|\mathbf{S}_{k,\ell}|^2)}{\mathbb{E}(\|(\mathbf{H}\mathbf{X} - \mathbf{S})_{k,\ell}\|_F^2) + \sigma_c^2}, \quad (5)$$

and so the rate of the k^{th} user is $R_k = \log_2(1 + \text{SINR}_k)$, following Shannon-theory. The MUI reflects a communication key performance indicator (KPI). Another important KPI is the PAPR is a waveform metric, which is the ratio of peak values to average power of that waveform. For example, a constant waveform enjoys a PAPR equal to one. The PAPR of a discrete time signal of NL samples is expressed as

$$\text{PAPR}(\mathbf{x}) = \frac{\max_{\ell=1 \dots NL} |\mathbf{x}(\ell)|^2}{\frac{1}{NL} \sum_{\ell=1}^{NL} |\mathbf{x}(\ell)|^2}. \quad (6)$$

As for sensing KPI, we adopt a similarity constraint between the designed waveform, and a desired radar waveform, such as a given chirp waveform. Let the reference radar waveform be denoted as \mathbf{x}_0 , hence a similarity constraint forms a sphere centered at the desired waveform \mathbf{x}_0 with radius ϵ ,

$$\mathbf{x} \in \mathcal{B}_\epsilon(\mathbf{x}_0) = \{\mathbf{x}, \|\mathbf{x} - \mathbf{x}_0\|^2 \leq \epsilon^2\}. \quad (7)$$

In short, the MUI, PAPR and the similarity constraints will serve as three KPIs to the formulation of our ISAC problem.

IV. ISAC WAVEFORM DESIGN FRAMEWORK

We formulate an optimization framework intended to maximize the total achievable rate of communication users, with sensing radar similarities and tunable PAPR. It is worth noting that, under a unit-energy constellation, maximizing SINR_k is equivalent of minimizing MUI_k . We propose the following MOO problem, where

$$(\mathcal{P}_{\text{MOO}}) : \begin{cases} \min_{\{\mathbf{x}\}} & [\|\mathbf{H}\mathbf{X} - \mathbf{S}\|_F^2, \ \|\mathbf{x} - \mathbf{x}_0\|^2, \ \text{PAPR}(\mathbf{x})] \\ \text{s.t.} & \|\mathbf{x}\|_F^2 = 1. \end{cases} \quad (8)$$

where $\mathbf{x} = \text{vec}(\mathbf{X})$. Note that in the above MOO, the aim is to find a waveform \mathbf{x} that joint minimizes the MUI, the radar similarity constraint and the PAPR. Said differently, we would like to obtain a waveform that is close to both radar and communication metrics, with a low PAPR. However, MOOs are usually complex to solve in real time [22]. As an alternative, we propose to minimize the MUI term, while bounding the radar similarity constraint and the PAPR. To this end, we have the following alternate optimization problem,

$$(\mathcal{P}) : \begin{cases} \min_{\{\mathbf{x}\}} & \|\mathbf{H}\mathbf{X} - \mathbf{S}\|_F^2 \\ \text{s.t.} & \text{PAPR}(\mathbf{x}) \leq \eta \\ & \mathbf{x} \in \mathcal{B}_\epsilon(\mathbf{x}_0), \\ & \|\mathbf{x}\|_F^2 = 1, \end{cases} \quad (9)$$

The problem is (9) is proposed as an alternative to the MOO in (8). The connection between (9) and (8) is that instead of jointly minimizing multi-user interference, radar chirp similarity, as well as the PAPR in (8), we only choose to minimize the multi-user interference, when the similarity and PAPR fall below certain pre-defined thresholds, controlled by ϵ and η . In [25], we show the equivalence of the problem (\mathcal{P}) to the following optimization problem

$$(\mathcal{P}') : \begin{cases} \min_{\{\mathbf{x}\}} & \|\mathbf{x} - \mathbf{x}_{\text{comm}}\|_F^2 \\ \text{s.t.} & \mathbf{x} \in \mathcal{B}_\epsilon(\mathbf{x}_0), \\ & \|\mathbf{x}\|_F^2 = 1, \\ & \mathbf{x}^H \mathbf{F}_n \mathbf{x} \leq \frac{\eta}{NL}, \quad \forall n \end{cases} \quad (10)$$

where $\mathbf{x}_{\text{comm}} = \text{vec}(\mathbf{H}^H(\mathbf{H}\mathbf{H}^H)^{-1}\mathbf{S})$. Furthermore, \mathbf{F}_n is a matrix of all-zeros, except for 1, which is positioned at its n^{th} diagonal entry. Note the equivalence between the PAPR constraint in (10) and that in (6), which is verified by designing an ISAC waveform \mathbf{x} under a norm-constraint, i.e. $\sum_{\ell=1}^{NL} |\mathbf{x}(\ell)|^2 = \|\mathbf{x}\|_F^2 = 1$, which when plugged in (6) gives

$$\max_{\ell=1 \dots NL} |\mathbf{x}(\ell)|^2 \leq \frac{\eta}{NL}, \quad (11)$$

which is satisfied when each and every element $|\mathbf{x}(\ell)|^2$ is upper-bounded by $\frac{\eta}{NL}$, hence the last constraint in (10). It can be easily noted that (\mathcal{P}') is non-convex due to the norm-equality constraint. Indeed, (\mathcal{P}') has several nice implications; the cost function could be interpreted as a similarity constraint between the waveform variable and a communication waveform, which is to be minimized. On the other hand, the first

constraint is a radar similarity constraint, which is controlled by input ϵ . The last two constraints are PAPR constraints. In the following section, we describe an ADMM procedure to solve (\mathcal{P}') in an efficient way.

V. ISAC DESIGN USING ADMM

The ADMM method has emerged as a powerful technique for large-scale structured optimization problems with applications in different fields, such as distributed and scalable processing [26] and image processing [27]. ADMM was initially devised as an iterative method for solving convex minimization problems by means of parallelization. However, it can also be applied in non-convex smooth optimization problems, such as group sparse problems [28]. Before tackling the augmented Lagrangian problem, we introduce auxiliary variables to the problem at hand as, thus problem (\mathcal{P}') is converted as

$$(\bar{\mathcal{P}}') : \begin{cases} \min_{\{\bar{\mathbf{x}}\}} & \|\bar{\mathbf{x}} - \bar{\mathbf{x}}_{\text{comm}}\|_F^2 \\ \text{s.t.} & \alpha = \bar{\mathbf{x}}, \quad \alpha^T \alpha = 1, \\ & \beta = \bar{\mathbf{x}} - \mathbf{x}_0, \quad \beta^T \beta \leq \epsilon^2, \\ & \gamma_n = \bar{\mathbf{F}}_n \bar{\mathbf{x}}, \quad \gamma_n^T \gamma_n \leq \frac{\eta}{NL}, \quad \forall n \end{cases} \quad (12)$$

Note that in the above steps, we have also converted the problem to a real-valued one, i.e. $\bar{\mathbf{x}} = [\text{Re}(\mathbf{x})^T \quad \text{Im}(\mathbf{x})^T]^T$. Likewise, the same conversion has been applied to $\bar{\mathbf{x}}_{\text{comm}}$ and $\bar{\mathbf{x}}_0$. Also, $\bar{\mathbf{F}}_n \in \mathbb{R}^{2NL \times 2NL}$ is an all-zero matrix except its n^{th} and $(NL + n)^{\text{th}}$ entries that are set to 1. Furthermore, given a penalty parameter $\rho > 0$, the augmented Lagrangian of the problem ($\bar{\mathcal{P}}'$) could be expressed as

$$\begin{aligned} \mathcal{L}_\rho(\bar{\mathbf{x}}, \alpha, \beta, \gamma_n, \mathbf{u}, \mathbf{v}, \mathbf{w}_n) &= \|\bar{\mathbf{x}} - \bar{\mathbf{x}}_{\text{comm}}\|_F^2 + \mathbf{u}^T (\bar{\mathbf{x}} - \alpha) + \mathbf{v}^T (\bar{\mathbf{x}} - \bar{\mathbf{x}}_0 - \beta) \\ &+ \sum_{n=1}^{NL} \mathbf{w}_n^T (\bar{\mathbf{F}}_n \bar{\mathbf{x}} - \gamma_n) + \frac{\rho}{2} \|\bar{\mathbf{x}} - \alpha\|^2 + \frac{\rho}{2} \|\bar{\mathbf{x}} - \bar{\mathbf{x}}_0 - \beta\|^2 \\ &+ \frac{\rho}{2} \sum_{n=1}^{NL} \|\bar{\mathbf{F}}_n \bar{\mathbf{x}} - \gamma_n\|^2, \end{aligned} \quad (13)$$

The variables are updated in following an iterative alternating pattern and over the regions of interest, namely

$$\mathcal{C}_\alpha = \{\alpha, \quad \alpha^T \alpha = 1\}, \quad (14a)$$

$$\mathcal{C}_\beta = \{\beta, \quad \beta^T \beta \leq \epsilon^2\}, \quad (14b)$$

$$\mathcal{C}_\gamma = \{\gamma, \quad \gamma^T \gamma \leq \frac{\eta}{NL}\}, \quad (14c)$$

In particular, at iteration m , the vector $\bar{\mathbf{x}}^{(m+1)}$ minimizes $\mathcal{L}_\rho(\bar{\mathbf{x}}, \alpha^{(m)}, \beta^{(m)}, \gamma_n^{(m)}, \mathbf{u}^{(m)}, \mathbf{v}^{(m)}, \mathbf{w}_n^{(m)})$. In the second update, given $\bar{\mathbf{x}}^{(m+1)}$, the vector $\alpha^{(m+1)}$ minimizes $\mathcal{L}_\rho(\bar{\mathbf{x}}^{(m+1)}, \alpha, \beta^{(m)}, \gamma_n^{(m)}, \mathbf{u}^{(m)}, \mathbf{v}^{(m)}, \mathbf{w}_n^{(m)})$. Then, given $\bar{\mathbf{x}}^{(m+1)}, \alpha^{(m+1)}, \beta^{(m+1)}$ minimizes $\mathcal{L}_\rho(\bar{\mathbf{x}}^{(m+1)}, \alpha^{(m+1)}, \beta, \gamma_n^{(m)}, \mathbf{u}^{(m)}, \mathbf{v}^{(m)}, \mathbf{w}_n^{(m)})$. The last update utilizes all the current values, i.e. $\bar{\mathbf{x}}^{(m+1)}, \alpha^{(m+1)}, \beta^{(m+1)}$ to update $\gamma_n^{(m+1)}$ by minimizing $\mathcal{L}_\rho(\bar{\mathbf{x}}^{(m+1)}, \alpha^{(m+1)}, \beta^{(m+1)}, \gamma_n, \mathbf{u}^{(m)}, \mathbf{v}^{(m)}, \mathbf{w}_n^{(m)})$. Last but

not least, before proceeding to iteration $m + 2$, the auxiliary variables are updated in a linear fashion as follows,

$$\mathbf{u}^{(m+1)} = \mathbf{u}^{(m)} + \rho(\bar{\mathbf{x}}^{(m+1)} - \alpha^{(m+1)}), \quad (15)$$

$$\mathbf{v}^{(m+1)} = \mathbf{v}^{(m)} + \rho(\bar{\mathbf{x}}^{(m+1)} - \mathbf{x}_0 - \beta^{(m+1)}), \quad (16)$$

$$\mathbf{w}_n^{(m+1)} = \mathbf{w}_n^{(m)} + \rho(\bar{\mathbf{F}}_n \bar{\mathbf{x}}^{(m+1)} - \gamma_n^{(m+1)}). \quad (17)$$

Algorithm 1 ADMM-based DFRC Waveform Design

INPUT $\mathbf{x}_0, \mathbf{H}, \mathbf{S}$

INIT $\alpha^{(0)} = \mathbf{0}, \beta^{(0)} = \mathbf{0}, \gamma_1^{(0)} = \gamma_2^{(0)} = \dots = \gamma_{NL}^{(0)} = \mathbf{0}$

INIT $\mathbf{u}^{(0)} = \mathbf{0}, \mathbf{v}^{(0)} = \mathbf{0}, \mathbf{w}_1^{(0)} = \mathbf{w}_2^{(0)} = \dots = \mathbf{w}_{NL}^{(0)} = \mathbf{0}$

SET $m \leftarrow 0, \mathbf{x}_{\text{comm}} = \text{vec}(\mathbf{H}^H (\mathbf{H}\mathbf{H}^H)^{-1} \mathbf{S})$

FORM $\bar{\mathbf{x}}_{\text{comm}} = [\text{Re}(\mathbf{x}_{\text{comm}})^T \quad \text{Im}(\mathbf{x}_{\text{comm}})^T]^T$

FORM $\bar{\mathbf{x}}_0 = [\text{Re}(\mathbf{x}_0)^T \quad \text{Im}(\mathbf{x}_0)^T]^T$

while $m < M_{\text{iter}}$ **do**

 Update $\mathbf{x}^{(m+1)}$ using equation (19)

 Update $\alpha^{(m+1)}$ using equation (20)

 Update $\beta^{(m+1)}$ using equation (21)

 Update $\gamma_1^{(m+1)} \dots \gamma_{NL}^{(m+1)}$ via equation (22)

 Update $\mathbf{u}^{(m+1)} \leftarrow \mathbf{u}^{(m)} + \rho(\bar{\mathbf{x}}^{(m+1)} - \alpha^{(m+1)})$

 Update $\mathbf{v}^{(m+1)} \leftarrow \mathbf{v}^{(m)} + \rho(\bar{\mathbf{x}}^{(m+1)} - \mathbf{x}_0 - \beta^{(m+1)})$

 Update $\mathbf{w}_n^{(m+1)} \leftarrow \mathbf{w}_n^{(m)} + \rho(\bar{\mathbf{F}}_n \bar{\mathbf{x}}^{(m+1)} - \gamma_n^{(m+1)})$

$m \leftarrow m + 1$

end while

return $\mathbf{x}^{(M_{\text{iter}})}$

To find $\bar{\mathbf{x}}^{(m+1)}$, we set the gradient of $\mathcal{L}_\rho(\bar{\mathbf{x}}, \alpha^{(m)}, \beta^{(m)}, \gamma_n^{(m)}, \mathbf{u}^{(m)}, \mathbf{v}^{(m)}, \mathbf{w}_n^{(m)})$ with respect to $\bar{\mathbf{x}}$ to zero,

$$\nabla_{\bar{\mathbf{x}}} \left[\mathcal{L}_\rho(\bar{\mathbf{x}}, \alpha^{(m)}, \beta^{(m)}, \gamma_n^{(m)}, \mathbf{u}^{(m)}, \mathbf{v}^{(m)}, \mathbf{w}_n^{(m)}) \right]_{\bar{\mathbf{x}} = \bar{\mathbf{x}}^{(m+1)}} = \mathbf{0}, \quad (18)$$

which gives.

$$\begin{aligned} \bar{\mathbf{x}}^{(m+1)} &= \frac{1}{2 + 3\rho} \left(2\bar{\mathbf{x}}_{\text{comm}} - \mathbf{u}^{(m)} - \mathbf{v}^{(m)} - \sum_{n=1}^{NL} \bar{\mathbf{F}}_n \mathbf{w}_n^{(m)} \right. \\ &\quad \left. + \rho\alpha^{(m)} + \rho(\bar{\mathbf{x}}_0 + \beta^{(m)}) + \rho \sum_{n=1}^{NL} \bar{\mathbf{F}}_n \gamma_n^{(m)} \right). \end{aligned} \quad (19)$$

For details in derivations, the reader is referred to [25]. Following similar steps, the update equations read

$$\alpha^{(m+1)} = \frac{\bar{\mathbf{x}}^{(m+1)} + \frac{1}{\rho} \mathbf{u}^{(m)}}{\|\bar{\mathbf{x}}^{(m+1)} + \frac{1}{\rho} \mathbf{u}^{(m)}\|}, \quad (20)$$

$$\beta^{(m+1)} = \begin{cases} \bar{\mathbf{x}}^{(m+1)} - \bar{\mathbf{x}}_0 + \frac{1}{\rho} \mathbf{v}^{(m)}, & \text{if } \in \mathcal{C}_\beta \\ \frac{\bar{\mathbf{x}}^{(m+1)} - \bar{\mathbf{x}}_0 + \frac{1}{\rho} \mathbf{v}^{(m)}}{\|\bar{\mathbf{x}}^{(m+1)} - \bar{\mathbf{x}}_0 + \frac{1}{\rho} \mathbf{v}^{(m)}\|}, & \text{otherwise.} \end{cases} \quad (21)$$

$$\gamma_n^{(m+1)} = \begin{cases} \bar{\mathbf{F}}_n \bar{\mathbf{x}}^{(m+1)} + \frac{1}{\rho} \mathbf{w}_n^{(m)}, & \text{if } \in \mathcal{C}_\gamma \\ \sqrt{\frac{\eta}{NL}} \frac{\bar{\mathbf{F}}_n \bar{\mathbf{x}}^{(m+1)} + \frac{1}{\rho} \mathbf{w}_n^{(m)}}{\|\bar{\mathbf{F}}_n \bar{\mathbf{x}}^{(m+1)} + \frac{1}{\rho} \mathbf{w}_n^{(m)}\|}, & \text{otherwise.} \end{cases} \quad (22)$$

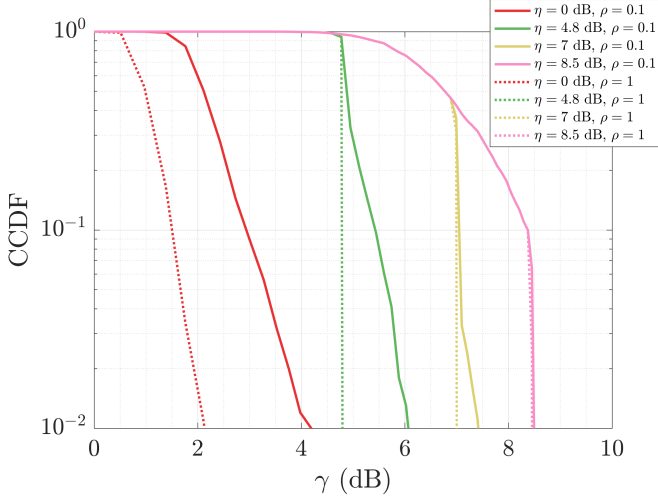


Fig. 2. The CCDF of the generated waveform described in Algorithm 1 for different values of η and ρ .

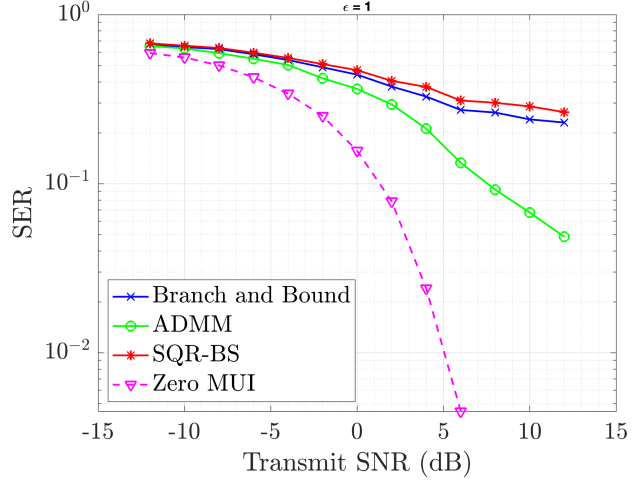


Fig. 4. The symbol error rate performance at $\epsilon = 1$ for $N = 5$ antennas and $K = 2$ communication users. The constellation utilized is a QPSK.

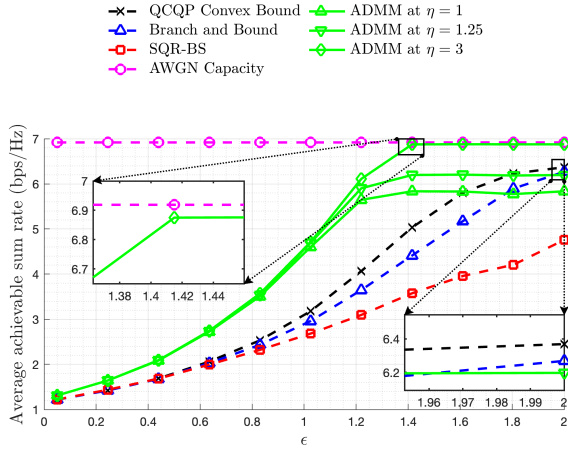


Fig. 3. Trade-off between the communication average achievable sum-rate per user and similarity waveform radar measure at SNR = 10 dB for $N = 4$ antennas and $K = 2$ communication users.

A summary of the proposed ADMM-based DFRC waveform design is summarized in **Algorithm 1**. Due to space restrictions in this manuscripts, the convergence analysis and complexity analysis of the proposed method can be found in our work in [25]. Also, note that this work assumes perfect channel state information, which is not the case in practice. A newly proposed algorithm is also found in [25] to cope with imperfect channel state information arising from practical scenarios, such as estimation errors.

VI. SIMULATION RESULTS

This section uses a variety of simulation results to show the effectiveness and trade-offs of the proposed ISAC-waveform design. The channel \mathbf{H} is drawn from a complex gaussian distribution and the desired constellation \mathcal{S} contains randomly selected quadrature amplitude modulation (QAM) symbols.

In Fig. 2, we plot the resulting complementary cumulative distribution function (CCDF) of the measured PAPR for different values of ρ, η . Note that the CCDF is computed as

$$\text{CCDF} \triangleq \Pr(\text{PAPR}(\mathbf{x}) > \gamma). \quad (23)$$

It is worth noting that increasing ρ results in a steeper cutoff of the PAPR CCDF most notable for larger values of η . For example, fixing the CCDF probability of 10^{-2} and a target PAPR of $\eta = 0\text{dB}$, we see that for $\rho = 0.1$, the required γ is $\gamma = 4.19\text{dB}$, whereas for $\rho = 1$, the γ is decreased by 2dB. On the other hand, tolerating a higher PAPR, this gap is reduced. Indeed, for $\eta = 4.8\text{dB}$, we can observe that for $\rho = 1$, the requirement is already satisfied at a CCDF probability of 10^{-2} , as opposed to when $\rho = 0.1$, we see that $\gamma = 6.11\text{dB}$, which reflects a gap of about 1.31dB. For a larger η , say $\eta = 7\text{dB}$, we see that the gap in γ is further reduced to 0.4dB between $\rho = 1$ and $\rho = 0.1$. Finally, this gap becomes negligible at $\eta = 8.5\text{dB}$. In Fig. 3, our goal is to investigate the trade-off between radar waveform similarity and communications sum-rate. The figure depicts the average achievable sum-rate as a function of ϵ for SNR = 10dB, $N = 4$ and $K = 2$. Fig. 3 delineates the average achievable sum-rate, as a function of ϵ at SNR = 10dB, $N = 4$ transmit antennas and $K = 2$ communication users. Also, some benchmarks are employed such as the successive quadratic constrained quadratic programming (QCQP) refinement (SQR) binary search (SQR-BS) algorithm proposed in [29], the BnB method [19], and the additive white Gaussian noise (AWGN) capacity. For $\epsilon < 1.6$, the performance of the proposed ADMM waveform design at $\eta = 1$ outperforms that of the QCQP convex bound and for $\epsilon < 1.8$ the ADMM method outperforms the BnB method. Note that all methods outperform the SQR-BS method, which agrees with the results in [19]. For a higher η , i.e. $\eta = 1.25$, we can observe that ADMM outperforms BnB for any ϵ . Additionally, we see that the ADMM achieves the AWGN capacity performance at $\epsilon > 1.42$ for $\eta = 3$. The capability

of PAPR adjustment explains the gain of the proposed ISAC ADMM-based design, which has a direct effect on sum-rate.

In Fig. 4, we now demonstrate the performance of communication for $\epsilon = 1$, which could be seen as "mid-way" between radar and communications. We are specifically interested with the symbol error rate (SER) performances, as a function of transmit SNR. We employ quadrature phase shift keying (QPSK) with random symbols streamed towards $K = 2$ communication users, via $N = 5$ transmit antennas at the DFRC BS. Now, we compare the SER of the proposed ADMM method compared to BnB, SQR-BS and a benchmark of zero MUI. For $\epsilon = 1$ and at a level of 10^{-1} SER, we see that the proposed ISAC waveform design based on ADMM is about 6dB away from the zero MUI performance. In addition, the proposed ADMM design outperforms BnB and SQR-BS by more than 7dB at a level of 10^{-1} SER. Therefore, this reveals the superiority of the proposed ADMM waveform design.

VII. CONCLUSIONS

In this paper, we have proposed an ISAC waveform design with desired radar waveform similarity, carrying multi-user communication information, and with adjustable PAPR. Indeed, this design is suitable for ISAC applications, where the IBO of the HPA is an important factor. Additionally, the trade-off between radar and communications has been revealed through simulations. Moreover, simulation results unveil the superiority of the proposed ADMM-based ISAC waveform design, as compared to state-of-the-art ISAC waveform.

REFERENCES

- [1] T. S. Rappaport, Y. Xing, O. Kanhere, S. Ju, A. Madanayake, S. Mandal, A. Alkhatieb, and G. C. Trichopoulos, "Wireless Communications and Applications Above 100 GHz: Opportunities and Challenges for 6G and Beyond," *IEEE Access*, vol. 7, pp. 78 729–78 757, 2019.
- [2] X. Cheng, Z. Huang, and L. Bai, "Channel Nonstationarity and Consistency for Beyond 5G and 6G: A Survey," *IEEE Communications Surveys & Tutorials*, vol. 24, no. 3, pp. 1634–1669, 2022.
- [3] A. Bazzi and M. Chafii, "Secure Full Duplex Integrated Sensing and Communications," *IEEE Transactions on Information Forensics and Security*, vol. 19, pp. 2082–2097, 2024.
- [4] Z. Xiao and Y. Zeng, "Waveform design and performance analysis for full-duplex integrated sensing and communication," *IEEE Journal on Selected Areas in Communications*, vol. 40, no. 6, pp. 1823–1837, 2022.
- [5] M. Chafii, L. Bariah, S. Muhaidat, and M. Debbah, "Twelve scientific challenges for 6g: Rethinking the foundations of communications theory," *IEEE Communications Surveys & Tutorials*, vol. 25, no. 2, pp. 868–904, 2023.
- [6] A. Bazzi and M. Chafii, "On Outage-based Beamforming Design for Dual-Functional Radar-Communication 6G Systems," *IEEE Transactions on Wireless Communications*, pp. 1–1, 2023.
- [7] D. Xu, X. Yu, D. W. K. Ng, A. Schmeink, and R. Schober, "Robust and Secure Resource Allocation for ISAC Systems: A Novel Optimization Framework for Variable-Length Snapshots," *arXiv preprint arXiv:2206.13307*, 2022.
- [8] A. Chowdhary, A. Bazzi, and M. Chafii, "On Hybrid Radar Fusion for Integrated Sensing and Communication," *IEEE Transactions on Wireless Communications*, pp. 1–1, 2024.
- [9] A. Bazzi and M. Chafii, "RIS-Enabled Passive Radar towards Target Localization," *arXiv preprint arXiv:2210.11887*, 2022.
- [10] A. W. Azim, A. Bazzi, R. Shubair, and M. Chafii, "Dual-Mode Chirp Spread Spectrum Modulation," *IEEE Wireless Communications Letters*, vol. 11, no. 9, pp. 1995–1999, 2022.
- [11] T. M. Pham, R. Bomfin, A. Nimr, A. N. Barreto, P. Sen, and G. Fettweis, "Joint Communications and Sensing Experiments Using mmWave Platforms," in *2021 IEEE 22nd International Workshop on Signal Processing Advances in Wireless Communications (SPAWC)*, 2021, pp. 501–505.
- [12] X. Hu, C. Masouros, F. Liu, and R. Nissel, "Low-PAPR DFRC MIMO-OFDM Waveform Design for Integrated Sensing and Communications," in *ICC 2022-IEEE International Conference on Communications*, IEEE, 2022, pp. 1599–1604.
- [13] A. Bazzi, D. T. Slock, and L. Meilhac, "Efficient maximum likelihood joint estimation of angles and times of arrival of multiple paths," in *2015 IEEE Globecom Workshops (GC Wkshps)*. IEEE, 2015, pp. 1–7.
- [14] Y.-C. Wang and Z.-Q. Luo, "Optimized iterative clipping and filtering for PAPR reduction of OFDM signals," *IEEE Transactions on communications*, vol. 59, no. 1, pp. 33–37, 2010.
- [15] G. Cui, H. Li, and M. Rangaswamy, "MIMO radar waveform design with constant modulus and similarity constraints," *IEEE Transactions on signal processing*, vol. 62, no. 2, pp. 343–353, 2013.
- [16] A. Bazzi and L. Meilhac, "Method for decoding an RF signal bearing a sequence of symbols modulated by cpm and associated decoder," Mar. 10 2022, US Patent App. 17/467,907.
- [17] G. Cui, X. Yu, V. Carotenuto, and L. Kong, "Space-time transmit code and receive filter design for colocated MIMO radar," *IEEE Transactions on Signal Processing*, vol. 65, no. 5, pp. 1116–1129, 2016.
- [18] A. I. Barros, J. Frenk, S. Schaible, and S. Zhang, "A new algorithm for generalized fractional programs," *Mathematical Programming*, vol. 72, no. 2, pp. 147–175, 1996.
- [19] F. Liu, L. Zhou, C. Masouros, A. Li, W. Luo, and A. Petropulu, "Toward dual-functional radar-communication systems: Optimal waveform design," *IEEE Transactions on Signal Processing*, vol. 66, no. 16, pp. 4264–4279, 2018.
- [20] H. Tuy, T. Hoang, T. Hoang, V.-n. Mathématicien, T. Hoang, and V. Mathematician, *Convex analysis and global optimization*. Springer, 1998.
- [21] A. De Maio, S. De Nicola, Y. Huang, Z.-Q. Luo, and S. Zhang, "Design of phase codes for radar performance optimization with a similarity constraint," *IEEE Transactions on Signal Processing*, vol. 57, no. 2, pp. 610–621, 2008.
- [22] E. Bjornson, E. A. Jorswieck, M. Debbah, and B. Ottersten, "Multiobjective signal processing optimization: The way to balance conflicting metrics in 5G systems," *IEEE Signal Processing Magazine*, vol. 31, no. 6, pp. 14–23, 2014.
- [23] J. A. Zhang, F. Liu, C. Masouros, R. W. Heath, Z. Feng, L. Zheng, and A. Petropulu, "An overview of signal processing techniques for joint communication and radar sensing," *IEEE Journal of Selected Topics in Signal Processing*, 2021.
- [24] S. K. Mohammed and E. G. Larsson, "Per-antenna constant envelope precoding for large multi-user MIMO systems," *IEEE Transactions on Communications*, vol. 61, no. 3, pp. 1059–1071, 2013.
- [25] A. Bazzi and M. Chafii, "On Integrated Sensing and Communication Waveforms with Tunable PAPR," *IEEE Transactions on Wireless Communications*, pp. 1–1, 2023.
- [26] T. Erseghe, "A distributed and scalable processing method based upon ADMM," *IEEE Signal Processing Letters*, vol. 19, no. 9, pp. 563–566, 2012.
- [27] S. Minaee and Y. Wang, "An ADMM approach to masked signal decomposition using subspace representation," *IEEE Transactions on Image Processing*, vol. 28, no. 7, pp. 3192–3204, 2019.
- [28] R. Chartrand and B. Wohlberg, "A nonconvex ADMM algorithm for group sparsity with sparse groups," in *2013 IEEE International Conference on Acoustics, Speech and Signal Processing*, 2013, pp. 6009–6013.
- [29] O. Aldayel, V. Monga, and M. Rangaswamy, "Successive QCQP refinement for MIMO radar waveform design under practical constraints," *IEEE Transactions on Signal Processing*, vol. 64, no. 14, pp. 3760–3774, 2016.